Co-existing of dressed non-linear gain and electromagnetically induced absorption

Dayu Zhu, Junling Che, Dan Zhang, Xiuxiu Wang, Zhenkun Wu, Yiqi Zhang, Yanpeng Zhang *

Key Laboratory for Physical Electronics and Devices of the Ministry of Education & Shaanxi Key Lab of Information Photonic Technique, Xi'an Jiaotong University, Xi'an 710049, China

ARTICLE INFO

ABSTRACT

The dressed parametric four-wave mixing (FWM) process has been investigated in hot atomic rubidium vapor. We use a strong pumping field to generate entangled photon pairs of spontaneous parametric FWM (SP-FWM) which can be enhanced by an external dressing effect. Seeding probe beam into the Stokes or anti-Stokes (SP-FWM) channel will form the parametric amplified FWM (PA-FWM) process, then the non-linear gain and electromagnetically induced absorption (EIA) are observed, caused by the internal dressing effect. However, with scanning of pumping field the absorbing background will vanish, which will result in drastic increase in PA-FWM signal gain.

© 2015 Elsevier B.V. All rights reserved.

1. Introduction

Atomic coherence in spontaneous parametric four-wave mixing (SP-FWM) [1,2] has been widely studied, due to the potential application in entangled and squeezed states [3] of quantum optics and cascaded nonlinear optics [4,5]. Applying a high power pumping beam into a thermal rubidium atomic vapor would induce a cycle of four transitions, which would stimulate the emission of entangled Stokes and anti-Stokes photons [3], thus the "double-Λ" FWM processes were introduced. For the process without seeding, the output is the two-mode squeezed state of FWM [6,7]. The instantaneous electric fields of the Stokes and anti-Stokes channels are averagely zero, while their fluctuations are quantum-correlated [4]. The mentioned process can serve as a linear phase-insensitive or phase-sensitive [8,9] amplifier by fitting experimental parameters, for the large scale of third-order nonlinear susceptibility will lead to an obvious quantum gain.

Recently, the results of seeding a weak probe beam into Stokes or Anti-Stokes channel have also attracted a lot of attention, where the non-input channel is called conjugate [10,11], and the twin beams are strongly correlated [12]. The process could be defined as Parametric Amplified Four-Wave Mixing (PA-FWM), then probe and conjugate beams can be both amplified [8] but with different multiples of Ω and $\Omega - 1$ [4], where the correlated pairs are with high generation rates and produce squeezed states with narrow bandwidths [13].

In this paper, we demonstrate an external dressing beam from the opposite direction of pumping field in the non-seeded system would produce strong dressing effect, which can modify the SP-FWM cone of pumping field. Moreover, instead of probe field, the pumping field is scanned for the first time in the PA-FWM process, which is advantageous over former experiments [9–11]. For one thing, the strong background will diminish by scanning dressing field, which allows the appearance of electromagnetically induced absorption (EIA) [14] in the resonant regions; for another, the values of observed gains would be greater, and there exist competition and transformation between EIA and gain process.
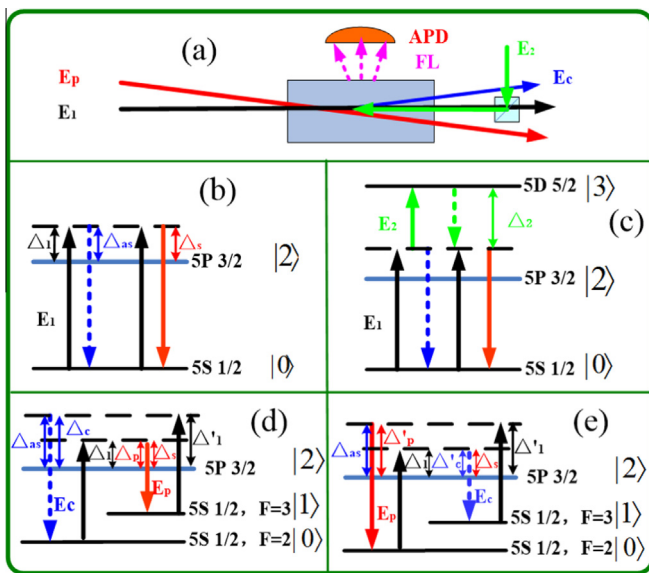
2. Experimental setup

A strong pumping beam ($\boldsymbol{E}_1$) from a Ti: sapphire laser is injected into the rubidium cell through polarization beam splitter (PBS) where ω_1, $\boldsymbol{k}_1$ and $\boldsymbol{G}_1$, are frequency, wave vector and Rabi

---

frequency of E_1, respectively. We use 780.2 nm wavelength and power up to 500 mw. The pumping field E_1 will generate two weak fields E_s and E_{as}, satisfying the phase matching conditions $k_s = 2k_1 - k_{as}$ and $k_{as} = 2k_1 - k_s$, respectively. The Stokes and anti-Stokes signals are detected by two balanced homodyne detectors, which are set at the same angle on both sides to the axis of pumping beam E_1. Moreover, an avalanche photodiode detector (APD) is placed near the cell for detecting fluorescence signal, and another detector is placed on the axis of pumping beam for detecting transmission signal. The resonant transition frequency between the ground state $5S_{1/2}$ ($|0\rangle$) and an excited state $5P_{3/2}$ ($|2\rangle$) is Ω_1. When a weak dressing field E_2 (ω_2, k_2, G_2 and 776.16 nm) is involved, the frequency between $5P_{3/2}$ ($|2\rangle$) and $5D_{5/2}$ ($|2\rangle$) is Ω_2. The dressing field will cause electromagnetically induced Transparency (EIT) and EIA on the basic resonant signal. The energy-level diagrams of the two experimental conditions are shown in Fig. 1 (b) and (c), which represent the resonant state.

Providing the weak horizontal polarization probe beam E_p (ω_p, k_p, G_p) of approximate 100 μw into the atomic vapor, which is excited by an external cavity diode laser(ECDL), a PA-FWM process will occur in the three level atomic configuration (Fig. 1(d) and (e)). The two ground fine states ($F = 2$, $|0\rangle$ and $F = 3$, $|1\rangle$) have a difference of 3 GHz in frequency. The probe (E_p) and the conjugate (E_c (ω_c, k_c, G_c)) satisfy the phase matching conditions $k_p = 2k_1 - k_c$ and $k_c = 2k_1 - k_p$, respectively. The intensity of probe signal is detected by the detector in Stokes or anti-Stokes channel. All beams are focused by lenses with focal length of 500 mm in front of the cell and the beams are intersected at the same central point inside the cell. The diameters of E_1 and E_p are 0.8 mm and 0.5 mm, respectively. The scale of 10 mm rubidium cell with Brewster's angle is wrapped by μ-metal and heated to 70–150 °C. By seeding E_p into the Stokes or anti-Stokes channel of the SP-FWM, the transmission signal in pumping field will be amplified due to the PA-FWM process. The observed output in probe field will result from the Raman absorption, EIA effect, parametrical amplification process and dressing effect by scanning E_p. Nonetheless, when scanning E_1 the absorbing background will vanish, which results in drastic increase in gain of signal.

3. Basic theory

3.1. SP-FWM without injection

When a pumping beam E_1 is detuned from $5S_{1/2}$ to $5P_{3/2}$ in the rubidium vapor, a conical emission is observed and twin photons are produced in output Stokes and anti-Stokes channels (denoted as a and b, respectively). The energy-level diagram is shown in Fig. 1(b). The Hamiltonian of such a phenomenon can be expressed as

$$\hat{H} = \frac{g}{\nu}\left(\hat{a}^+\hat{b}^+ + \hat{a}\hat{b}\right) \tag{1}$$

where $\hat{a}^+\hat{b}^+$ is the creation (annihilation) operator that acts on the electromagnetic excitation of the Stokes channel, whereas $\hat{a}\hat{b}$ acts on the anti-Stokes channel, ν is the group velocity of the light in the nonlinear medium. $g = |\chi^{(3)}E_1E_1| = |N\mu_{10}^2\rho_{s/as}^{(3)}/\hbar\varepsilon_0 G_{s/as}|$ is the pumping parameter of the amplifier, which depends on the nonlinearity $\chi^{(3)}$ and the amplitude of pumping field E_1. Unlike nonlinear crystal, the nonlinearity $\chi^{(3)}$ of such medium is a function of the density matrix elements described by their perturbation chains $\rho_{00}^{(0)} \xrightarrow{\omega_1} \rho_{20}^{(1)} \xrightarrow{\omega_{as}} \rho_{00}^{(2)} \xrightarrow{\omega_1} \rho_{20(s)}^{(3)}$ (Stokes signal) and $\rho_{00}^{(0)} \xrightarrow{\omega_1} \rho_{20}^{(1)} \xrightarrow{\omega_s} \rho_{00}^{(2)} \xrightarrow{\omega_1} \rho_{20(as)}^{(3)}$ (anti-Stokes signal) via the Liouville pathway [10] and can be written as

$$\rho_{20(as)}^{(3)} = -iG_sG_1^2 / \left(d_{20}d_{00(s)}d'_{20(s)}\right), \tag{2a}$$

$$\rho_{20(s)}^{(3)} = -iG_{as}G_1^2 / \left(d_{20}d_{00(as)}d'_{20(as)}\right), \tag{2b}$$

where $d_{20} = \Gamma_{20} - i\Delta_1$, $d_{00(s)} = \Gamma_{00} - i(\Delta_1 - \Delta_s)$, $d_{00(as)} = \Gamma_{00} - i(\Delta_1 - \Delta_{as})$, $d'_{20(s)} = \Gamma_{20} - i(2\Delta_1 - \Delta_s)$, $d'_{20(as)} = \Gamma_{20} - i(2\Delta_1 - \Delta_{as})$, $G_i = \mu_{ij}E_{ij}/\hbar$ ($i,j = s, as, c, p$) is the Rabi frequency, $\Gamma_{ij} = (\Gamma_i + \Gamma_j)/2$ is the decoherence rate between $|i\rangle$ and $|j\rangle$; Δ_i is the detuning between the resonant transition frequency Ω_i and the laser frequency ω_i of E_i, denoted as $\Delta_i = \omega_i - \Omega_i$. In this experiment, the SP-FWM process occurs at the resonant detuning $\Delta_1 = \Delta_s = \Delta_{as}$, shown in Fig. 1(b). When Stokes and anti-Stokes fields propagate in the nonlinear medium, the numbers of photons measured at the two channels are

$$\langle\hat{a}_{out}^+\hat{a}_{out}\rangle = \frac{1}{2}\left[\cos\left(2t\sqrt{AB}\sin\frac{\varphi_1+\varphi_2}{2}\right) + \cosh\left(2t\sqrt{AB}\cos\frac{\varphi_1+\varphi_2}{2}\right)\right] \times \frac{A}{B}, \tag{3a}$$

$$\langle\hat{b}_{out}^+\hat{b}_{out}\rangle = \frac{1}{2}\left[\cos\left(2t\sqrt{AB}\sin\frac{\varphi_1+\varphi_2}{2}\right) + \cosh\left(2t\sqrt{AB}\cos\frac{\varphi_1+\varphi_2}{2}\right)\right] \times \frac{B}{A}, \tag{3b}$$

where A and B are the moduli [4], φ_1 and φ_2 are the phase angles of $\rho_{21(s)}^{(3)} = Ae^{i\varphi_1}$ and $\rho_{20(as)}^{(3)} = Be^{i\varphi_2}$, respectively. Therefore, the outputs of Stokes and anti-Stokes channels of SP-FWM are at the same value as

$$\Omega = \frac{1}{2}\left[\cos\left(2t\sqrt{AB}\sin\frac{\varphi_1+\varphi_2}{2}\right) + \cosh\left(2t\sqrt{AB}\cos\frac{\varphi_1+\varphi_2}{2}\right)\right]. \tag{4}$$

If we inject E_2 into the SP-FWM as a dressing field, the ladder-type three-level atomic configuration is formed, as shown in Fig. 1(c). Thus, Eq. (2) will be rewritten as

$$\rho_{20(as)}^{(3)} = -iG_sG_1^2 / \left[d_{00(s)}d'_{20(s)}(G_2^2/d_{30} + d_{20})\right], \tag{5a}$$

$$\rho_{20(s)}^{(3)} = -iG_{as}G_1^2 / \left[d_{00(as)}d'_{20(as)}(G_2^2/d_{30} + d_{20})\right], \tag{5b}$$

Fig. 1. (a) Experimental setup. E_1: pumping field; E_2: dressing field; E_p: probe field; E_c: conjugate field; FL: fluorescence signal; APD: avalanche photodiode detector. (b) Energy-level diagram with seeding E_1 only. (c) Energy-level diagram with seeding E_1 and E_2. (d) Energy-level diagram with E_1 and seeding E_p into Stokes channel. (e) Energy-level diagram with E_1 and seeding E_p into anti-Stokes channel.

where $d_{30} = (\Gamma_{30} - i(\Delta_1 + \Delta_2))$. The dressing effect of $\boldsymbol{E}_2$ is observed not only in Stokes and anti-Stokes channels but also in the pumping field $\boldsymbol{E}_1$. The Stokes and anti-Stokes channels are also influenced by the leaking light from $\boldsymbol{E}_1$, which is dominated by $\rho_{20}^{(1)}$. It can be expressed as $\rho_{20}^{(1)} = iG_1/d_{20}$ and the perturbation chain can be written as $\rho_{00}^{(0)} \xrightarrow{\omega_1} \rho_{20}^{(1)}$. When both the internal and external dressing effects of $\boldsymbol{E}_1$ and $\boldsymbol{E}_2$ are considered, the equation could be rewritten as

$$\rho_{20}^{(1)} = \frac{iG_1}{d_{20} + G_1^2/\left(\Gamma_{00} + G_1^2/d_{20}\right) + G_2^2/d_{30}}. \tag{6}$$

Since $\rho_{20(s)}^{(3)}$ and $\rho_{20(as)}^{(3)}$ are equal in both Eqs. (2) and (5) ($\rho_{20(s)}^{(3)} = \rho_{20(as)}^{(3)} = \rho_{20}^{(3)}$), the intensity of Stokes and anti-Stokes signal can be expressed as $I_{(s/as)} \propto \left(I_0 - \text{Im}(\rho_{20}^{(1)}) + \left|\rho_{20}^{(3)}\right|^2\right)$, where $\text{Im}\left(\rho_{20}^{(1)}\right)$ causes EIA or EIT and $\left|\rho_{20}^{(3)}\right|^2$ causes gain.

3.2. PA-FWM with injection

3.2.1. Stokes PA-FWM

The SP-FWM signal can be amplified through seeding probe beam $\boldsymbol{E}_p$ (energy level diagrams Fig. 1(d) and (e)). The phenomenon can be observed as PA-FWM. If $\boldsymbol{E}_p$ is seeded into Stokes channel (Fig. 1(d)), the perturbation chain can be expressed as $\rho_{11}^{(0)} \xrightarrow{\omega_1} \rho_{21}^{(1)} \xrightarrow{\omega_c} \rho_{01}^{(2)} \xrightarrow{\omega_1} \rho_{21(s)}^{(3)}$ (Stokes channel), and the density matrix element is written as:

$$\rho_{21(s)}^{(3)} = -iG_c G_1^2/(d_{21}d_{01}d_{21}'), \tag{7}$$

where $d_{01} = \Gamma_{01} - i(\Delta_1' - \Delta_c)$, $d_{21} = \Gamma_{21} - i\Delta_1'$ and $d_{21}' = \Gamma_{21} - i(\Delta_1 + \Delta_1' - \Delta_c)$. If the dressing effects of $\boldsymbol{E}_1$, $\boldsymbol{E}_p$ are involved then Eq. (7) should be rewritten as

$$\rho_{21(s)}^{(3)} = \frac{-iG_c G_1^2}{d_{21}'\left[d_{01} + G_1^2/d_{21}' + G_c^2/d_{21} + G_1^2/d_{02}\right]}$$
$$\times \frac{1}{d_{21} + G_1^2/\Gamma 11 + G_1^2/\Gamma_{22} + G_1^2/d_{01}' + G_c^2/d_{01}}. \tag{8}$$

where $d_{02} = \Gamma_{02} - i\Delta_c$, $d_{10}' = \Gamma_{10} - i(\Delta_1 - \Delta_1')$ and $d_{01}' = \Gamma_{01} - i(\Delta_1' - \Delta_1)$. The satisfied two-photon conditions are written as $\Delta_p - \Delta_s = 0$, $\Delta_c - \Delta_{as} = 0$, $\Delta_1 - \Delta_s = 0$, $\Delta_1' - \Delta_{as} = 0$ and $\Delta_p - \Delta_c + 3\text{ GHz} = 0$ (Fig. 1(d)). The PA-FWM signal of probe field $\boldsymbol{E}_p$ is composition of Stokes $\rho_{21(s)}^{(3)}$ and probe $\rho_{20}^{(1)}$, i.e. $I_p \propto \left(I_0 - \text{Im}(\rho_{20}^{(1)}) + \left|\rho_{21(s)}^{(3)}\right|^2\right)$ (EIA and dressed gain), where

$$\rho_{20}^{(1)} = \frac{iG_p}{\Gamma_{21} - i\Delta_p + G_p^2/\Gamma_{21} + G_p^2/\Gamma_{22} + G_1^2/d_{01}'' + G_1^2/d_{22}}, \tag{9}$$

$d_{01}'' = \Gamma_{01} - i(\Delta_p - \Delta_1)$, $d_{22} = \Gamma_{22} - i(\Delta_p - \Delta_1')$ and $G_p \propto \sqrt{2/\varepsilon_0 c \hbar} N \mu^2 \rho_{21(s)}^{(3)}$. The corresponding perturbation chain of probe beam $\boldsymbol{E}_p$ is $\rho_{00}^{(0)} \xrightarrow{\omega_p} \rho_{20}^{(1)}$.

3.2.2. Anti-Stokes PA-FWM

The anti-Stokes signal also can be amplified by seeding probe beam $\boldsymbol{E}_p$ into the anti-Stokes channel (Fig. 1(e)), according to perturbation chain $\rho_{00}^{(0)} \xrightarrow{\omega_1} \rho_{20}^{(1)} \xrightarrow{\omega_c} \rho_{10}^{(2)} \xrightarrow{\omega_1} \rho_{20(as)}^{(3)}$ (anti-Stokes signal), we have

$$\rho_{20(as)}^{(3)} = -iG_c G_1^2/(d_{20}d_{10}''d_{20}''), \tag{10}$$

where $d_{20}'' = \Gamma_{20} - i(\Delta_1 + \Delta_1' - \Delta_c')$, $d_{10}'' = \Gamma_{10} - i(\Delta_1 - \Delta_c')$. If the dressing effects of $\boldsymbol{E}_1$, $\boldsymbol{E}_p$ are involved then Eq. (10) can be rewritten as

$$\rho_{20(as)}^{(3)} = \frac{-iG_c G_1^2}{d_{20}'''\left[d_{10}'' + G_1^2/d_{20}''' + G_c^2/d_{20} + G_1^2/d_{12}'\right]}$$
$$\times \frac{1}{d_{20} + G_1^2/\Gamma 00 + G_1^2/\Gamma_{22} + G_1^2/d_{10}' + G_c^2/d_{10}''}, \tag{11}$$

where $d_{12}' = \Gamma_{12} - i\Delta_c'$. The satisfied two-photon conditions could be written as $\Delta_p' - \Delta_{as} = 0$, $\Delta_c' - \Delta_s = 0$, $\Delta_1 - \Delta_S = 0$, $\Delta_1' - \Delta_{as} = 0$, and $\Delta_p' - \Delta_c' - 3\text{ GHz} = 0$ (Fig. 1(e)). The PA-FWM signal of probe field is a composition of anti-Stokes $\rho_{20(as)}^{(3)}$ and probe $\rho_{21}^{(1)}$, i.e., $I_p \propto \left(I_0 - \text{Im}(\rho_{21}^{(1)}) + \left|\rho_{20(as)}^{(3)}\right|^2\right)$ (EIA and dressed gain), where

$$\rho_{21}^{(1)} = \frac{iG_p}{\Gamma_{20} - i\Delta_p' + Gp^2/\Gamma_{00} + Gp^2/\Gamma_{22} + G_1^2/d_{00}' + G_c^2/d_{10}'''}, \tag{12}$$

$d_{10}''' = \Gamma_{10} - i\left(\Delta_p' - \Delta_1'\right)$, $\qquad d_{00}' = \Gamma_{00} - i\left(\Delta_p' - \Delta_1\right)$, and $G_p \propto \sqrt{2/\varepsilon_0 c \hbar} N \mu^2 \rho_{20(as)}^{(3)}$.

Consequently, due to the photon number of seeded signal $n \gg 1$, the measured numbers of such an amplifier (with $\boldsymbol{E}_p$ seeded) at probe and conjugate channels are

$$\langle \hat{a}_{out}^+ \hat{a}_{out} \rangle_p = \frac{1}{2}\left[\cos\left(2t\sqrt{AB}\sin\frac{\varphi_1+\varphi_2}{2}\right) + \cosh\left(2t\sqrt{AB}\cos\frac{\varphi_1+\varphi_2}{2}\right)\right]|\alpha|^2, \tag{13a}$$

$$\langle \hat{b}_{out}^+ \hat{b}_{out} \rangle_c = \frac{1}{2}\frac{B}{A}\left[\cosh\left(2t\sqrt{AB}\cos\frac{\varphi_1+\varphi_2}{2}\right) - \cos\left(2t\sqrt{AB}\sin\frac{\varphi_1+\varphi_2}{2}\right)\right]|\alpha|^2, \tag{13b}$$

where $|\alpha|^2 = \frac{\pi\varepsilon_0 c\hbar}{2\omega_1}\left(\frac{G_{Probe}r}{\mu_{10}}\right)^2$ denotes the intensity of the seeded field, r is the radius of beam $\boldsymbol{E}_p$. Thus, the gain of each channel can be calculated as

$$\Omega_p = \frac{1}{2}\left[\cos\left(2t\sqrt{AB}\sin\frac{\varphi_1+\varphi_2}{2}\right) + \cosh\left(2t\sqrt{AB}\cos\frac{\varphi_1+\varphi_2}{2}\right)\right], \tag{14a}$$

$$\Omega_c = \frac{1}{2}\frac{B}{A}\left[\cos\left(2t\sqrt{AB}\sin\frac{\varphi_1+\varphi_2}{2}\right) + \cosh\left(2t\sqrt{AB}\cos\frac{\varphi_1+\varphi_2}{2}\right)\right]. \tag{14b}$$

4. Experimental results

4.1. SP-FWM without injection

At first, we study degenerate SP-FWM process in Fig. 2. In Fig. 2(a1)–(a3), the pumping beam $\boldsymbol{E}_1$ is on while probe beam $\boldsymbol{E}_p$ and dressing beam $\boldsymbol{E}_2$ are blocked. The vertical dotted lines in Fig. 2 exhibits the corresponding relation between the dressed suppressed dip in fluorescence channel and EIT in Stokes and anti-Stokes channels. Later, the dressing beam $\boldsymbol{E}_2$ is injected as shown in Fig. 2(b1)–(b3). The dressing beam $\boldsymbol{E}_2$ causes a new ladder-type three-level atomic configuration. The EIA of pumping channel itself has been observed, as well as the corresponding EIT in Stokes channel. All the fluorescence, Stokes and anti-Stokes signals appear in the resonant window $\Delta_1 = \Delta_s = \Delta_{as}$.

Fig. 2(a1) shows signals in fluorescence channel and the intensity can be expressed as $I_{FL} \propto \text{Im}(\rho_{22}^{(2)})$, where $\rho_{22}^{(2)} = -G_1^2/\left[d_{20}\left(\Gamma_{22} + G_1^2/d_{20}\right)\right]$, and perturbation chain is $\rho_{00}^{(0)} \xrightarrow{\omega_1} \rho_{20}^{(1)} \xrightarrow{\omega_1} \rho_{22}^{(2)}$. The term $d_{20} = \Gamma_{20} - i\Delta_1$ in $\rho_{22}^{(2)}$ is responsible for the broad fluorescence signal, and the dressing term G_1^2/d_{20} causes the suppressed dip in fluorescence signal as shown in Fig. 2(a1). There are two series of broad fluorescence signal and dressed suppression dip, which correspond to ^{87}Rb ($F = 2$) and ^{85}Rb ($F = 3$). The double dips of fluorescence signal can be observed clearly in ^{87}Rb ($F = 2$) when the frequency difference between its
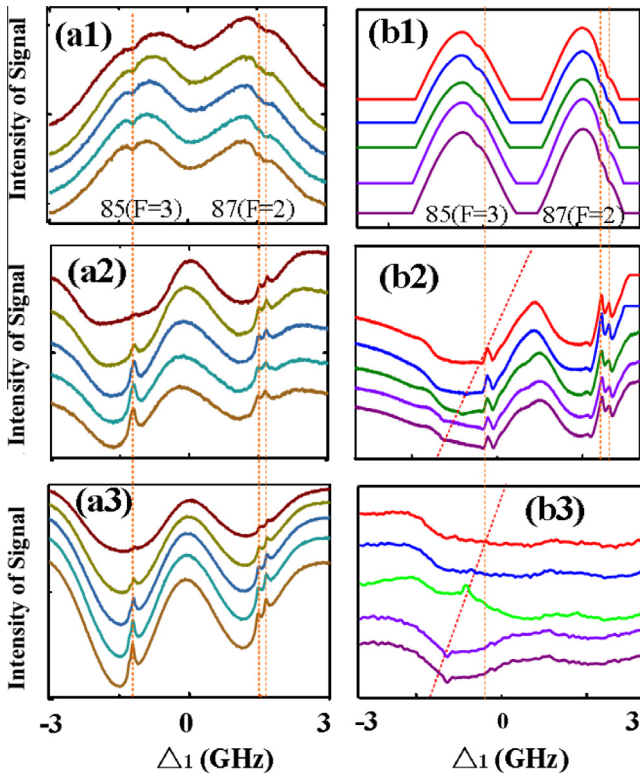
Fig. 2. (a1)–(a3) Measured signal intensities with only turning on pumping beam E_1 at different pumping powers. (a1) Signals in fluorescence channel. (a2) Signals in Stokes channel. (a3) Signals in anti-Stokes channel. (b1)–(b3) Measured signal intensities with turning on pumping field E_1 and dressing field E_2 at different pumping powers. (b1) Signals in fluorescence channel. (b2) Signals in Stokes channel. (b3) Transmission signals in pumping channel. With the rising of pumping power, all the signals are getting more obvious.

upper hyperfine energy levels ($F' = 3$ to $F' = 4$) is 267 MHz. While for ^{85}Rb ($F = 3$), the frequency difference between its upper hyperfine energy levels is only 121 MHz, which is too small to distinguish double dips. The double EITs also appear at respective positions in Stokes and anti-Stokes channels of ^{87}Rb ($F = 2$) (Fig. 2 (a2) and (a3)).

Since Stokes and anti-Stokes signals are quantitatively the same ($\rho^{(3)}_{20(s)} = \rho^{(3)}_{20(as)} = \rho^{(3)}_{20}$), shown as $I_{(s/as)} \propto \left(I_0 - \text{Im}(\rho^{(1)}_{20}) + \left| \rho^{(3)}_{20} \right|^2 \right)$. The first order term d_{20} of $\rho^{(1)}_{20}$ (Eq. (6)) can explain the broad absorption dip in Stokes (Fig. 2(a2) and (b2)) and anti-Stokes channels (Fig. 2(a3)). While the dressing term $G_1^2 / \left(\Gamma_{00} + G_1^2/d_{20} \right)$ in $\rho^{(1)}_{20}$ causes EIT peak, d_{20} of $\rho^{(3)}_{20}$ (Eq. (2)) attributes to the SP-FWM peak, and they overlap together. It can be found that the contribution of $\rho^{(3)}_{20}$ is much higher than that EIT peak of $\rho^{(1)}_{20}$ due to square of d_{20} in $\rho^{(3)}_{20}$. Hence the SP-FWM peak is dominated by $\rho^{(3)}_{20}$.

When E_2 is injected into the Rb vapor, the signals in Fig. 2(a1)–(a3) also could be observed in Fig. 2(b1)–(b3), but E_2 has dressing effect on them. The external dressing term $d_{30} = G_2^2/(\Gamma_{30} - i(\Delta_1 + \Delta 2))$ of E_2 will be applied in Eqs. (5) and (6), where Δ_2 is the detuning of E_2. So d_{30} can be used to explain the dressing effect of Stokes signal (Eq. (5)) and pumping signal (Eq. (6)), as shown in Fig. 2 (b2) and (b3), respectively. When we change Δ_2, the dressed EIA dip of pumping channel transits to dressed EIT peak, and the signal moves as denoted by the decline dotted line (Fig. 2(b3)). The corresponding dip or peak also moves with the same speed in Stokes channel (Fig. 2(b2)). The crossing point of the vertical and decline dotted line shows the E_2-dressed EIT peak moves to the position of E_1-dressed SP-FWM peak in

Fig. 2(b2) and (b3). Then the E_1-dressed-peak will be enhanced by the E_2-dressed-peak. Since E_1 calls for internal dressing, E_2 calls for external dressing, the enhancement peak can be controlled by internal and external dressing effects.

4.2. PA-FWM with injection

Next, we investigate the PA-FWM process (i.e. SP-FWM process with seeding E_p in Fig. 1(a)) in Fig. 3 and subsequent figures, whose signal is the combination of EIA dip and gain peak. From an overall perspective, we observe three non-resonant signals in Fig. 3, which correspond to ^{87}Rb ($F = 2$), ^{85}Rb ($F = 3$) and ^{85}Rb ($F = 2$) on the frequency spectrum (from left to right in Fig. 3(b1)), respectively.

In Fig. 3, we study the EIA dip (caused by $\text{Im}\left(\rho^{(1)}_{21}\right)$ or $\text{Im}\left(\rho^{(1)}_{20}\right)$) and gain peak (caused by $\left| \rho^{(3)}_{20(as)} \right|^2$ or $\left| \rho^{(3)}_{21(s)} \right|^2$) via changing temperature. Such signals convert from purely EIA to the combination of peak and EIA, finally only the gain peak appears (from left to right in Fig. 3(b1)). Since $\Delta_1 = \Delta_s = \Delta_{as}$ is not the quantum window in PA-FWM process, the resonant EIT of SP-FWM process observed in Fig. 2 would not appear in the E_p seeded system.

The Stokes PA-FWM signals of ^{87}Rb($F = 2$) [^{85}Rb($F = 3$)] raised at the conditions of $\Delta_p - \Delta_S = 0$, $\Delta_c - \Delta_{as} = 0$, $\Delta_1 - \Delta_S = 0$, $\Delta'_1 - \Delta_{as} = 0$ and $\Delta_p - \Delta_c + 3$ GHz $= 0$ (Fig. 1(d)). The value of Stokes signal can be shown by the format $I_p \propto \left(I_0 - \text{Im}\left(\rho^{(1)}_{20}\right) + \left| \rho^{(3)}_{21(s)} \right|^2 \right)$, while the two-photon term $d_{01} = \Gamma_{01} - i(\Delta'_1 - \Delta_c)$ in $\rho^{(3)}_{21(s)}$ (Eq. (7)) can illustrate the gain peak
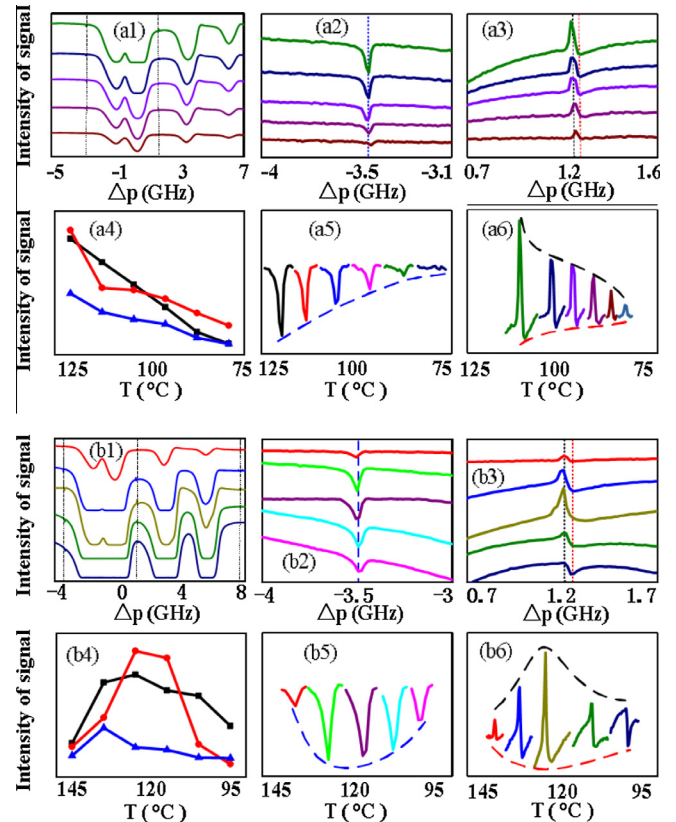
Fig. 3. (a1)–(a6) Temperature changing from 125 °C to 75 °C. (a1) Complete signal curves. (a2) Signals of ^{87}Rb($F = 2$). (a3) Signals of ^{85}Rb ($F = 3$). (a4) Dependences of all the signals' evolution, where the line with squares shows the gain of ^{85}Rb($F = 3$), line with dots shows the dip of ^{85}Rb($F = 3$) and line with triangles shows dip of ^{87}Rb ($F = 2$). (a5) Joint figures of the dips in (a2). (a6) Joint figures of the peaks and dips in (a3). (b1)–(b6) Same as (a1)–(a6) but the temperature changing from 95 °C to 145 °C.

in Stokes window, while dressing term G_1^2/d_{01}'' in $\rho_{20}^{(1)}$ (Eq. (9)) is responsible for the EIA dip in the same window, where $d_{01}'' = \Gamma_{01} - i(\Delta_p - \Delta_1)$. There is only EIA dip in ^{87}Rb($F = 2$) (Fig. 3 (a2) and (a5)), which means the existence of $\rho_{20}^{(1)}$ with $\rho_{21(s)}^{(3)} \sim 0$; but there exist both EIA dip and gain peak of ^{85}Rb($F = 3$) (Fig. 3 (a3) and (a6)). This is because of the distinguished energy levels of isotope ^{85}Rb and ^{87}Rb, which results in dressing switch of suppression and enhancement [15].

Meanwhile, the gain peak of ^{85}Rb($F = 2$) in the right of Fig. 3(b1) appears when probe beam $\boldsymbol{E}_p$ is seeded into anti-Stokes channel. The peak raises at the conditions of $\Delta_p' - \Delta_{as} = 0$, $\Delta_c' - \Delta_S = 0$, $\Delta_1 - \Delta_S = 0$, $\Delta_1' - \Delta_{as} = 0$, and $\Delta_p' - \Delta_c' - 3$ GHz $= 0$ (Fig. 1(e)). Thus the value of Im($\rho_{21}^{(1)}$) (Eq. (12)) is smaller whereas $\left|\rho_{20(as)}^{(3)}\right|^2$ (Eq. (10)) predicts a larger one, due to $I_p \propto \left(I_0 - \text{Im}(\rho_{21}^{(1)}) + \left|\rho_{20(as)}^{(3)}\right|^2\right)$. Therefore, the suppressed EIA dip almost disappears but the gain peak is more dramatic, which satisfies the enhancement condition. The difference between ^{85}Rb($F = 2$) and ^{85}Rb($F = 3$) means that the differing energy levels [16] would lead to the break of suppressed condition.

Since temperature stands for atomic density to an extent, higher vapor density means longer propagation distance, so temperature could represent propagation distance. Due to $G_P \propto \sqrt{2/\varepsilon_0 c \hbar} N \mu^2 \rho_{21(s)}^{(3)}$ or $G_P \propto \sqrt{2/\varepsilon_0 c \hbar} N \mu^2 \rho_{20(as)}^{(3)}$, the change of temperature will have direct impact on EIA dip and gain peak. In Fig. 3(a1)–(a6), the temperature drops from 125 °C to 75 °C. The EIA of ^{87}Rb($F = 2$) (Fig. 3(a5)) as well as the combination of EIA and gain of ^{85}Rb($F = 3$) (Fig. 3(a6)) all decrease linearly when temperature falls down. While on the contrary, in Fig. 3(b1)–(b6) the temperature raises from 95 °C to 145 °C, the intensities of signals change non-linearly. The EIA of ^{87}Rb($F = 2$) (Fig. 3(b5)) and the combination of EIA and gain of ^{85}Rb($F = 3$) (Fig. 3(b6)) grow to a peak value at the temperature of about 121 °C and then start to fall to a lower level. That is to say, the saturated turning points of Fig. 3 (a4) and (b4) are divergent. Compared to Fig. 3(a4), in Fig. 3(b4) the temperature (propagation distance) is relatively higher and with stronger power of $\boldsymbol{E}_1$. The two FWM beams of Stokes and anti-Stokes channels can be matched well under the same ultraslow group velocity by the dressing control [17,18]. So the energy of Stokes field could transfer to anti-Stokes field under such a condition, and then the intensity of Stokes signals would decrease in Fig. 3(b4) due to intense dressing effects.

Then in Fig. 4 we only investigate the Stokes PA-FWM signal of ^{85}Rb($F = 3$) according to energy-level diagram shown in Fig. 1(d). When we inject the probe beam $\boldsymbol{E}_p$ into the Rb vapor, there appears EIA dip and gain peak in $\Delta_1 - \Delta_p = 0$ window, which is controlled by Δ_1, power of pumping and probe field.

In Fig. 4(a1), the increasing Δ_1 causes the gain peak and EIA dip to decrease and they move together with the same speed, which testimonies the Stokes PA-FWM signal is the combination of $\rho_{21(s)}^{(3)}$ and $\rho_{20}^{(1)}$ given as $I_p \propto \left(I_0 - \text{Im}\left(\rho_{20}^{(1)}\right) + \left|\rho_{21(s)}^{(3)}\right|^2\right)$. The gain peak appears due to the two-photon term d_{01} in $\rho_{21(s)}^{(3)}$ (Eq. (7)), and EIA dip appears due to the dressing term G_1^2/d_{01}'' in $\rho_{20}^{(1)}$ (Eq. (9)). Hence, scanning Δ_p versus different Δ_1 would make the EIA dip and gain peak move together in the same window $\Delta_1 - \Delta_p = 0$. Moreover, the increase of Δ_1 means the decreasing of $\left|\rho_{21(s)}^{(3)}\right|^2$ for the one-photon term d_{21}, so we can see the process of gain peak intensity decreases in Fig. 4(a2) and (a3). However, the drop of gain peak is more drastic than that of EIA dip. This can be explained that Δ_1 in Eq. (7) appears three times as product
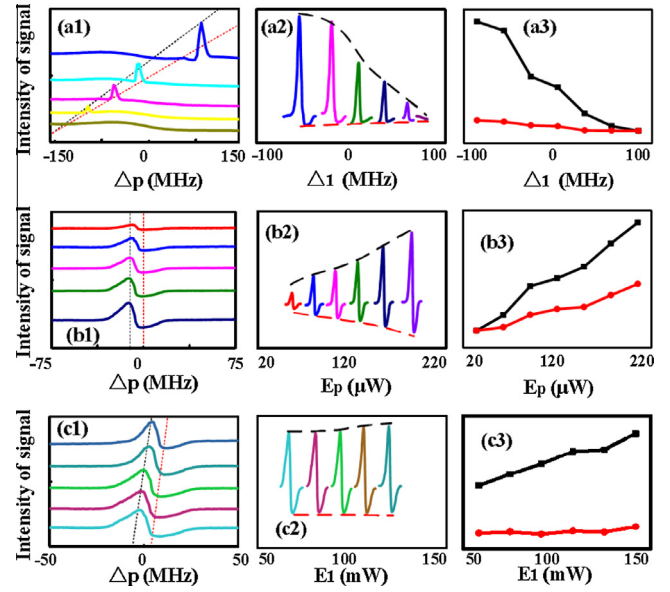

Fig. 4. Measured gain and dip of ^{85}Rb($F = 3$) signal in probe channel versus Δ_p at different Δ_1, probe power and pumping power, respectively. (a1)–(a3) Changing detuning (Δ_1) of $\boldsymbol{E}_1$. (a1) Experimental data curves of ^{85}Rb($F = 3$) signal. (a2) Joint figures of the signals in (a1). (a3) Dependence of the signals' evolution, where the line with squares shows the gain of ^{85}Rb($F = 3$) and line with dots shows the dip of ^{85}Rb($F = 3$). (b1)–(b3) Changing the power of $\boldsymbol{E}_p$. (c1)–(c3) Changing the power of $\boldsymbol{E}_1$.

form then by squaring it $\left(\left|\rho_{21(s)}^{(3)}\right|^2\right)$ we obtain sixth power. Therefore the change of Δ_1 will be amplified to sixth effect which causes the gain peak sensitive to detuning. However, Δ_1 in $\rho_{20}^{(1)}$ only appears as the first power in dressing term G_1^2/d_{01}'', so the EIA dip is not strongly influenced by Δ_1.

If we improve the power of probe beam, G_p, the signals are enlarged as in Fig. 4(b1)–(b3). In $\rho_{21(s)}^{(3)}$, the change of $\boldsymbol{G}_p$ can influence the Stokes signal linearly. Whereas in $\rho_{20}^{(1)}$ (Eq. (9)) $\boldsymbol{G}_p$ exists both in the denominator (dressing term $G_p^2/\Gamma_{11} + G_p^2/\Gamma_{22}$) and numerator ($iG_p$), so the change of EIA dip is much gentler than gain peak. Finally the power of pumping field, $\boldsymbol{G}_1$, is varied in Fig. 4(c1)–(c3). When we increase $\boldsymbol{G}_1$, the value of $\rho_{21(s)}^{(3)}$ (Eq. (7)) rises, and the value of $\rho_{20}^{(1)}$ (Eq. (9)) falls because $\boldsymbol{G}_1$ exists in the denominator of $\rho_{20}^{(1)}$ (dressing term $G_1^2/d_{01}'' + G_1^2/d_{22}$), but numerator of $\rho_{21(s)}^{(3)}$ (G_1^2), both are in square form. The result is that the gain peak is getting larger, but the change of EIA dip is not that obvious, as shown in Fig. 4(c2) and (c3).

Finally, in Fig. 5 the Stokes PA-FWM [EIA dip ($\rho_{20}^{(1)}$ in Eq. (9)) and gain peak ($\rho_{21(s)}^{(3)}$ in Eq. (7))] process is studied by scanning pumping field $\boldsymbol{E}_1$ at different Δ_p for the first time. Compared to Figs. 3 and 4, the advantages of scanning $\boldsymbol{E}_1$ are the absence of the broad absorption dips ($\rho_{20}^{(1)}$ without dressing), and Stokes PA-FWM signals at resonant positions could be observed, and PA-FWM is much more dramatic at non-resonant positions. Because the intensity of $\boldsymbol{E}_1$ is much larger than $\boldsymbol{E}_p$, $\boldsymbol{E}_1$ provides stronger dressing effect than $\boldsymbol{E}_p$. Thus, PA-FWM is more obvious versus scanning $\boldsymbol{E}_1$ due to the free of broad absorption [19].

The assertion can be made that the strong Stokes PA-FWM signal corresponding to ^{87}Rb($F = 2$), ^{85}Rb($F = 3$) and ^{85}Rb($F = 2$) lead to the co-existence of both EIA dip and gain peak, which are raised by $\rho_{20}^{(1)}$ (Eq. (9)) and $\rho_{21(s)}^{(3)}$ (Eq. (7)), respectively. The Stokes windows
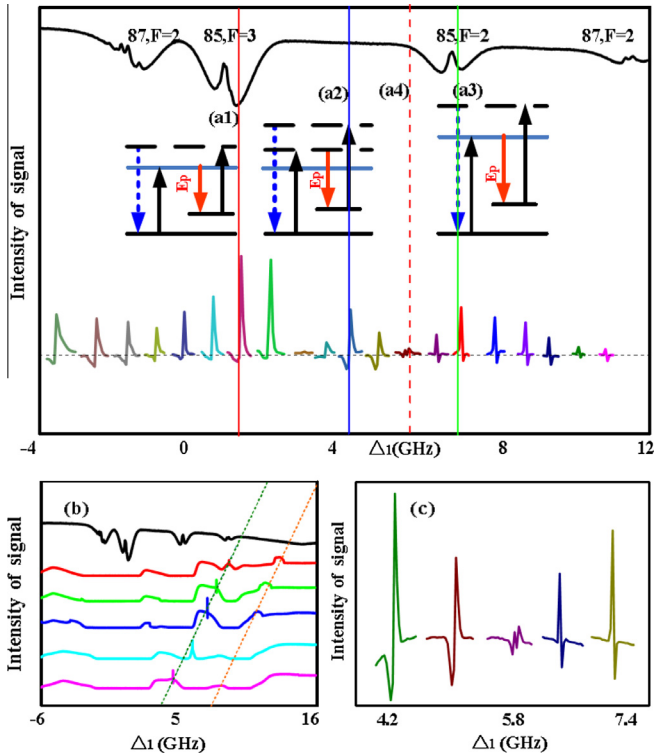
Fig. 5. (a1)–(a4) Intensity evolutions of Stokes signals in the probe channel versus Δ_1 at different Δ_p. (b) Spectra and the moving tendency of Stokes signals. (c) Transition of gain peak and EIA dip of Stokes signals.

are the same to those in Fig. 3. But the difference is that in Fig. 3, Stokes PA-FWM signal of ^{87}Rb($F = 2$) only appears as EIA dip, ^{85}Rb($F = 2$) as only gain peak. In addition, compared to Fig. 2, we could also observe Stokes signals at the resonant position of ^{85}Rb ($F = 3$) and ^{85}Rb($F = 2$). However, the main disparity is that in Fig. 2 there are SP-FWM peaks in broad absorption dip; while in Stokes PA-FWM process of Fig. 5, the PA-FWM signals appear as the combination of EIA dip and gain peak, for absence of broad absorption dip (Fig. 5(b)). The disparity is caused by seeding probe beam E_p. What's more, Fig. 5(b) denotes degenerate PA-FWM (right decline dotted line) and Stokes non-degenerate PA-FWM signal (left decline dotted line), which move with the same speed via modulation of Δ_p. For gain peak appears due to the two-photon term d_{01} in $\rho_{21(s)}^{(3)}$ (Eq. (7)), and EIA dip appears due to the dressing term G_1^2/d_{01}'' in $\rho_{20}^{(1)}$ (Eq. (9)), scanning Δ_1 versus different Δ_p would cause the values of EIA dip and gain peak change, and they could move together due to the common term $\Delta_1 - \Delta_p$, similar to Fig. 4(a1). The EIA dips and gain peaks (Fig. 5(a)) at non-resonant positions are all much more dramatic than those in Figs. 3 and 4.

The intensities of PA-FWM signals change periodically because of three highest positions of the signals (Fig. 5(a1)–(a3)). The first maximum appears at ^{85}Rb($F = 3$) with resonant ($\Delta_1 = 0$) of pumping beam E_1, corresponding to the left energy configuration of Fig. 5(a1). We did not observe the resonant PA-FWM signal in Figs. 3 and 4, because when probe field E_p is scanned, the broad absorption dip would wash out the PA-FWM signal at the resonant position. The maximum appears when the frequencies match precisely. The second maximum position is also at ^{85}Rb($F = 3$) (middle energy configuration Fig. 5(a2)), while the detuning is 1.2 GHz, satisfying the same Stokes window ($\Delta_1 - \Delta_p = 0$) in Fig. 4. It can be considered that this gain signal is the same to the one discussed

attentively in Fig. 4. The last maximum in Fig. 5(a3) corresponds to the right energy configuration, which parallels ^{85}Rb($F = 2$) with resonant ($\Delta_1 = 0$) pumping field E_1. Compared to the pure gain peak ^{85}Rb($F = 2$) PA-FWM signal stated in Fig. 3, the co-existence of both EIA dip and gain peak are observed in Fig. 5(a3). This is because $\rho_{20}^{(1)}$ (Eq. (9)) gets to maximum at $\Delta_1 = \Delta_p = 0$, while in Fig. 3 the Stokes window $\Delta_1 - \Delta_p = 0$ rises when Δ_1 is about 1.2 GHz. Thus $\rho_{20}^{(1)}$ in Fig. 5 is larger than that in Fig. 3, which causes the appearance of EIA dip in Fig. 5.

Lastly, Fig. 5(c) shows that when the detuning of E_p changes linearly, the structures of the signals change from left-dip and right-peak to left-peak and right-dip. The turning point can be seen as the mass center between ^{85}Rb($F = 2$) and ^{85}Rb($F = 3$) [19], shown as vertical dot line (Fig. 5(a4)). Due to the competition of gain and dip, the intensity of PA-FWM signal comes to a minimum at this symmetric center (Fig. 5(c)).

5. Conclusion

We have observed conical emission of output twin photons of SP-FWM process first by seeding a pumping beam into rubidium atomic vapor, later by injecting another beam which acts as external dressing field. Enhancement of dressed SP-FWM peak in Stoke channel is attributed to dressing field. Further the enhancement peak can be controlled by dressing effect. While PA-FWM system is achieved by seeding another probe beam individually into output channels of SP-FWM. The results of parametric amplification and gain process of Stokes are attributed to extrinsic parameters of seeding (changing detuning and power) and intrinsic parameter (changing temperature). Such results will help to understand the fundamental of coupled multi-level atom system, which could have potential applications in quantum information processing.

Acknowledgements

References

[1] M.D. Lukin, P.R. Hemmer, M. Löffler, M.O. Scully, Resonant enhancement of parametric processes via radiative interference and induced coherence, Phys. Rev. Lett. 81 (1998) 2675–2678.

[2] M.D. Lukin, A.B. Matsko, M. Fleischhauer, M.O. Scully, Quantum noise and correlations in resonantly enhanced wave mixing based on atomic coherence, Phys. Rev. Lett. 82 (1999) 1847–1850.

[3] V. Boyer, A.M. Marino, R.C. Pooser, P.D. Lett, Entangled images from four-wave mixing, Science 321 (2008) 544–547.

[4] H.B. Zheng, X. Zhang, Z.Y. Zhang, Y.L. Tian, H.X. Chen, C.B. Li, Y.P. Zhang, Parametric amplification and cascaded-nonlinearity processes in common atomic system, Sci. Rep. 3 (2013) 1885.

[5] H.X. Chen, Y.Q. Zhang, X. Yao, Z.K. Wu, X. Zhang, Y.P. Zhang, M. Xiao, Parametrically amplified bright-state polariton of four- and six-wave mixing in an optical ring cavity, Sci. Rep. 4 (2014) 3619.

[6] H.P. Yuen, J.H. Shapiro, Generation and detection of two-photon coherent states in degenerate four-wave mixing, Opt. Lett. 4 (1979) 334–336.

[7] R.E. Slusher, L.W. Hollberg, B. Yurke, J.C. Mertz, J.F. Valley, Observation of squeezed states generated by four-wave mixing in an optical cavity, Phys. Rev. Lett. 55 (1985) 2409–2412.

[8] N.V. Corzo, A.M. Marino, K.M. Jones, P.D. Lett, Noiseless optical amplifier operating on hundreds of spatial modes, Phys. Rev. Lett. 109 (2012) 043602.

[9] R.C. Pooser, A.M. Marino, V. Boyer, K.M. Jones, P.D. Lett, Low-noise amplification of a continuous variable quantum state, Phys. Rev. Lett. 103 (2009) 010501.

[10] C.F. McCormick, V. Boyer, E. Arimondo, P.D. Lett, Strong relative intensity squeezing by four-wave mixing in rubidium vapor, Opt. Lett. 32 (2007) 178–180.

[11] M. Jasperse, L.D. Turner, R.E. Scholten, Relative intensity squeezing by four-wave mixing with loss: an analytic model and experimental diagnostic, Opt. Express. 19 (2011) 3765–3774.

[12] H. Wu, M. Xiao, Bright correlated twin beams from an atomic ensemble in the optical cavity, Phys. Rev. A 80 (2009) 063415.

[13] C. Liu, J. Jing, Z. Zhou, R.C. Pooser, F. Hudelist, L. Zhou, W. Zhang, Realization of low frequency and controllable bandwidth squeezing based on a four-wave-mixing amplifier in rubidium vapor, Opt. Lett. 36 (2008) 2979–2981.

[14] J. Dimitrijević, D. Arsenović, B.M. Jelenković, Intensity dependence narrowing of electromagnetically induced absorption in a Doppler-broadened medium, Phys. Rev. A 76 (2007) 013836.

[15] Z.G. Wang, P.Y. Li, Z.Y. Zhang, C.J. Lei, F.R. Lei, H.X. Chen, Y.P. Zhang, Comparison of ultranarrow fluorescence and four-wave mixing in electromagnetically induced transparency windows, IEEE Photon. J. 5 (2013) 2600311.

[16] U. Khadka, H. Zheng, M. Xiao, Four-wave-mixing between the upper excited states in a ladder-type atomic configuration, Opt. Express 20 (2012) 6204–6214.

[17] Y.P. Zhang, A.W. Brown, M. Xiao, Matched ultraslow propagation of highly efficient four-wave mixing in a closely cycled double-ladder system, Phys. Rev. A 74 (2006) 053813.

[18] Y.P. Zhang, B. Anderson, M. Xiao, Efficient energy transfer between four-wave-mixing and six-wave-mixing processes via atomic coherence, Phys. Rev. A 77 (2008) 061801.

[19] P.Y. Li, H.B. Zheng, Y.Q. Zhang, J. Sun, C.B. Li, G.P. Huang, Z.Y. Zhang, Y.Y. Li, Y.P. Zhang, Controlling the transition of bright and dark states via scanning dressing field, Opt. Mater. 35 (2013) 1062–1070.